Charge-density analysis of $YBa_2Cu_3O_{6.98}$. Comparison of theoretical and experimental results

Thomas Lippmann,[a]* Peter Blaha,[b] Niels H. Andersen,[c] Henning F. Poulsen,[c] Thomas Wolf,[d] Jochen R. Schneider[e] and Karl-Heinz Schwarz[b]

[a]GKSS Forschungszentrum, Max-Planck-Strasse 1, 21502 Geesthacht, Germany, [b]Technical University Wien, Institute for Material Chemistry, 1060 Wien, Austria, [c]Risø National Laboratory, Materials Research Department, 4000 Roskilde, Denmark, [d]Forschungszentrum Karlsruhe, IFP, 76021 Karlsruhe, Germany, and [e]Hamburger Synchrotronstrahlungslabor HASYLAB at Deutsches Elektronen-Synchrotron DESY, Notkestrasse 85, 22603 Hamburg, Germany. Correspondence e-mail: thomas.lippmann@gkss.de

Using high-energy synchrotron radiation, structure factors of $YBa_2Cu_3O_{6.98}$ were measured at $\lambda = 0.124$ Å. Charge densities were derived using generalized structure factors and *VALRAY* and compared to densities refined from theoretical structure factors, which were calculated using the LAPW method and *WIEN2k*. Refinement agreement indices were $R(F) = 0.0047$ for the experimental and 0.0023 for the theoretical data set, respectively. Experimental and theoretical results generally agree well. A topological analysis shows that the structure is mainly ionic but depletion of charge density between Cu and O gives hints for covalency and confirms the general consensus of hole localization in these bonds.

1. Introduction

After the discovery of the high-T_c superconductors, significant theoretical and experimental efforts were made to determine their crystalline and intricate electronic structure in order to unravel the mechanism underlying high-T_c superconductivity, *e.g.* Pickett (1989). Theoretical investigations of the electronic structure are in principle only limited by the applied models and methods and by computer power and these have been significantly improved in the last years, *e.g.* Madsen *et al.* (2001). On the other hand, experimental investigations are limited both by the quality of the crystals and by the method used to investigate the atomic and electronic structures. In general, the development of methods for crystal growth of pure and monodomain high-T_c superconductors with sufficient sample sizes is still under progress, but nowadays for a few high-T_c superconductor structures it is already possible to grow monodomain and untwinned samples of up to a few hundred µm (Wolf, 1996), which is a reasonable size for charge-density investigations.

$YBa_2Cu_3O_{6+x}$ is one of the most investigated high-T_c superconductors because of the relatively high phase-transition temperature of about 90 K. Moreover, the phase diagram indicates the existence of either a superconducting ortho-rhombic or an antiferromagnetic tetragonal structure depending on the oxygen content x of the sample, which can easily be adjusted by gas volumetric technique (Andersen *et al.*, 1990). $YBa_2Cu_3O_{6+x}$ crystallizes in a distorted perovskite structure (Fig. 1), *i.e.* the structure can be considered as consisting of several layers stacked along the c axis: a copper—

oxygen (basal) layer at fractional coordinate $z = 0$ [including atoms Cu(1), O(1), O(5)], a barium—oxygen layer at $z \approx 0.17$ [Ba, O(4)], a second copper—oxygen layer at about $z = 0.365$ [O(2), O(3), Cu(2)], and the Y atom at $z = 0.5$. The lattice
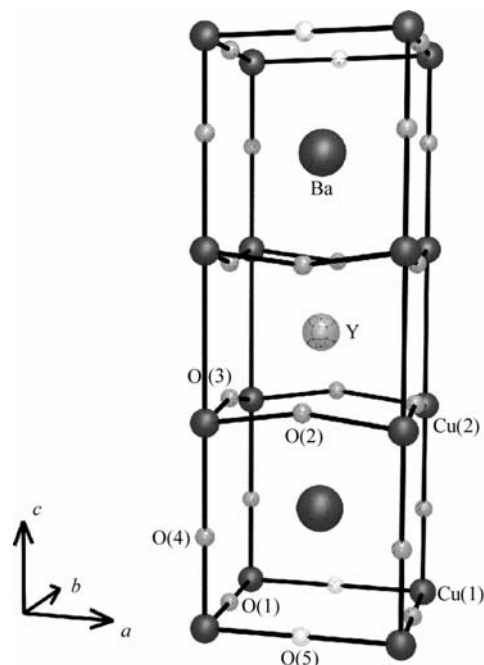
Figure 1
The structure of $YBa_2Cu_3O_{6.98}$. Y: large bright sphere, Ba: large dark spheres, Cu: small dark spheres; O: small bright spheres.

constants are about $a_0 = 3.82$, $b_0 = 3.88$ and $c_0 = 11.68$ Å in the orthorhombic structure, depending on the oxygen content x. In the fully oxygen loaded structure ($x \approx 1$), the O(5) site is unoccupied.

In the past, reliable experimental charge densities of high-T_c superconductors were very difficult to obtain (Sasaki *et al.*, 1992; Buttner *et al.*, 1992; Sullivan *et al.*, 1993; Jang *et al.*, 1996) because the irregular shape of the investigated samples and the presence of the heavy elements Y and Ba made proper absorption corrections impossible. Moreover, using conventional X-ray photon energy, the data suffered from severe extinction. The availability of high-energy synchrotron radiation, however, now allows high-quality structure factors to be measured in reasonable time periods of a few days. So far, the method has been tested on cuprite, Cu_2O (Lippmann & Schneider, 2000*a,b*, LSa and LSb hereafter) and stishovite, SiO_2 (Kirfel *et al.*, 2001), yielding data that turned out to be well suited for charge-density studies and topological analyses.

In this paper, we present results of both an experimental and a theoretical study of $YBa_2Cu_3O_{6.98}$. The theoretical study has been performed using linear augmented plane-wave (LAPW) density-functional calculations (Schwarz & Blaha, 1996) and the algorithms implemented in the program *WIEN2k* (Blaha *et al.*, 2001). Thus, the paper is organized as follows: After a short description of the sample growth characteristics, the experiment and the calculation method, results of both theoretical and experimental structure-factor refinements are presented. Characteristics and details of theoretical and experimental charge densities are shown, discussed and compared. Additionally, results of topological analyses are presented.

2. Sample growth and preparation

$YBa_2Cu_3O_{6.98}$ single crystals were grown in self-flux starting from Y_2O_3, $BaCO_3$ and CuO powders with a purity better than 99.99%. After several calcination steps, the powders were melted in a Y-stabilized ZrO_2 crucible at 1293 K. Crystal growth took place during slow cooling to 1209 K at a cooling rate of 0.8 K h^{-1}. At the end of the growth process, the remaining flux was decanted within the furnace and the crystals were cooled down to room temperature. In a second step, the crystals were oxidized by annealing them between 873 and 653 K in an atmosphere of 1 bar O_2 over 750 h. A crystal of suitable size and without twins was selected by inspection in polarized light.

3. Experimental

The experiment was performed at room temperature on the triple-crystal diffractometer (Bouchard *et al.*, 1997) at the HASYLAB beamline BW5 during DORIS III five-bunch mode operation, which corresponds to a beam current varying between 150 and 80 mA. The experimental set-up for the structure-factor measurements at BW5 is described in detail in LSa. An annealed silicon 111 crystal (rocking curve FWHM $\approx$ 5″ at 100 keV) was used as monochromator. The energy was

Table 1
Crystallographic and data-collection parameters and anomalous-dispersion corrections.

Lattice constants of $YBa_2Cu_3O_{6.98}$	$a_0 = 3.823$ (1), $b_0 = 3.887$ (1), $c_0 = 11.680$ (1)
Space group	$Pmmm$
Sample size	Slice, $\approx$200 μm diameter <20 μm thickness
Beam size	1×1 mm
Monochromator	Si 111, FWHM: 5.8″
Detector aperture	12 mm $\times$ 12 mm
Detector–sample distance	1200–1340 mm
Temperature	295 K (ambient)
Energy	99.49 keV
Wavelength	0.124 Å
Scattering geometry	Horizontal
Scan mode	ω step scans, bisecting mode
Steps/scan	61
$\Delta\omega$	$0.01°$
Scan speed	$0.6°$ min^{-1}
Test reflection	156
Test interval	30 min
No. of reflections	2052
No. of uniques	1026
$(\sin\Theta/\lambda)_{max}$	1.05 Å^{-1}
$R_{int}(F^2)$	0.0038
Anomalous-dispersion corrections [e atom^{-1}] ($E = 100$ keV) (Chandler, 1995)	$f'(Ba) = 0.359$, $f''(Ba) = 0.639$, $f'(Y) = 0.163$, $f''(Y) = 0.151$, $f'(Cu) = 0.067$, $f''(Cu) = 0.043$, $f'(O) = 0.001$, $f''(O) = 0.000$

roughly fixed to 100 keV, and then exactly measured using a perfect silicon crystal and the method of King & Finger (1979), which yielded 99.49 keV. The scattering plane was horizontal. The data were recorded using a germanium solid-state detector for the sample signal and an NaI scintillation counter for monitoring the incident beam. Since the triple-crystal diffractometer at BW5 was originally not designed for standard four-circle data collection, we improved the instrument by fast motors at the Eulerian cradle, SINCOS MSO power supplies, VME electronics and a fast Linux PC, so that up to 1500 reflections can now be measured per day at the beamline.

Prior to the data collection, the crystal was checked for its monodomain character and for twinning by taking rotation photographs with an image plate. No indications for polydomains or for twinning were found in any of these photographs. A further check was performed by fitting Gaussians to the reflection profiles.[1] About 100 reflections of both high and low order were arbitrarily selected here, and all profiles were properly fitted using single Gaussians. Hence, the crystal was assumed to be monodomain.

Table 1 summarizes the crystallographic and data-collection parameters. The maximum count rate was limited to 60 000 counts s^{-1} by the use of various well defined iron blocks as attenuators for the strong reflections. Short-term beam instabilities were checked by remeasuring various reflections and were not observed. Long-term beam drifts were checked by measuring a test reflection each 30 min. The deviations of these test intensities were found to be less than 2% during a complete DORIS run. In the case of drifts, a cubic spline was

---

[1] The 'quasi-Gaussian' shape of the profiles is mainly determined by the mosaicity of the monochromator crystal.

fitted to the test intensities and the data were subsequently corrected for.

4. Data reduction

The derivation of structure factors $|F_{obs,H}|$ of each reflection H from the integrated intensities $I_{int,H}$ was performed using

$$I_{int,H} = L_H P_H A_H T_H |F_{obs,H}|^2, \tag{1}$$

where L is the Lorentz, P the polarization, A the absorption and T the thermal diffuse scattering (TDS) correction.

For the polarization corrections, a degree of 90% linear horizontally polarized radiation was assumed according to earlier polarization measurements performed at BW5 (Poulsen & Neufeind, 1995). In contrast to the experiment on cuprite (see LSa), the absorption correction could not be neglected here, since the linear absorption coefficient of $YBa_2Cu_3O_{6.98}$ is 6.35 cm^{-1} at 100 keV, which is larger than for cuprite, and our sample was not a sphere but a slice of about 200 µm diameter and a thickness of less than 20 µm. However, the absorption correction was not a severe problem because the orientation of the crystallographic c_0 axis of the sample was well defined, i.e. perpendicular to the flat surface. Although the edges of the sample were somewhat irregular, the approximation of these edges by a polygon did not introduce significant errors into the structure factors.

The absorption correction for a reflection H was calculated by integration over the crystal volume V_c according to

$$A_H = \left[V_c^{-1} \int_{V_c} \exp(-\mu t_H)\, dV \right]^{-1}, \tag{2}$$

where t_H denotes the beam path inside the crystal and has to be calculated according to the crystal shape and orientation with respect to the beam. The maximum correction $A_{max} = 1.114$ was found for reflection 002, and the minimum was $A_{min} = 1.013$ for 100.

The TDS correction was applied using the program *TDSCOR* (Eichhorn, 1982) and elastic constants provided by Menon & Eldhose (1992). The maximum intensity correction was about 3% for the highest-order reflections and refinement tests yielded no significant differences using either the corrected or uncorrected data. Additional profile analyses of high-order reflections also yielded no significant indications for TDS.

Averaging a total of 2052 reflections yielded 1026 unique reflections with an internal consistency of 0.0038.

5. LAPW calculations

The theoretical calculations for stoichiometric $YBa_2Cu_3O_7$ have been performed using the full potential 'augmented plane wave + local orbitals' (APW+lo) method as implemented in the *WIEN2k* code (Blaha *et al.*, 2001). These calculations are based on density functional theory (DFT) and use the local density approximation (LDA) (Perdew & Wang, 1992). We used a well converged basis set of more than 3000

Table 2
Data sets and refined models.

Denotation	Explanation
ESF/IAM	Independent atom model (IAM) refinement of 1026 experimental structure factors (ESF)
ESFHO/IAM	IAM refinement of 553 high-order structure factors of ESF ($\sin \Theta/\lambda > 0.8$ Å^{-1})
ESF/HFW	Multipole refinement of ESF using expansions of Hartree–Fock wavefunctions (HFW) (Clementi & Roetti, 1974; Thakkar, 2001)
TSF/HFW	Multipole refinement of theoretical structure factors (TSF) using HFW
CSF/HFW	Multipole refinement of ESF using HFW (oxygen radial parameters constrained to each other)
ESF/EXP	Multipole refinement of ESF using single exponential functions (EXP)
TSF/EXP	Multipole refinement of TSF using EXP
CSF/EXP	Multipole refinement of ESF using EXP (oxygen radial parameters constrained to each other)
ND	Neutron diffraction results (Casalta *et al.*, 1996)

APWs with additional local orbitals for Y 3s, 3p; Ba 5p; Cu 3p; and O 2s states.

We calculated theoretical X-ray structure factors by a Fourier transformation of the self-consistent electron density. These theoretical structure factors were then used in the refinements using *VALRAY* and these results are denoted by TSF in this paper. For other comparisons of theoretical and experimental structure factors of light elements, the reader is referred to e.g. Howard *et al.* (1995), Volkov *et al.* (2000) or Bytheway *et al.* (2002).

In order to estimate the influence of the fitting procedure (and the truncation in reciprocal space), we calculate the bond critical points (b.c.p., see topological analysis below) once from the fitted data but also directly from the theoretical charge density using a recently developed program (Sofo & Fuhr, 2001), which may serve as benchmark for the quality and reliability of the fitting procedure.

It is well known that LDA is not accurate enough to describe the antiferromagnetic insulating ground state of $YBa_2Cu_3O_6$ nor the electric field gradient (EFG) at the planar Cu(2) site in this cuprate (Schwarz *et al.*, 1990). Thus, it is very likely that the theoretical charge distribution around the Cu(2) site is not properly described in theory based on LDA. [Note that the EFG and thus the (non-spherical) charge distribution around all other sites agree very well with the experimental NQR data.] For this reason, we performed additional calculations using the LDA+U method (Novak *et al.*, 2001). This method treats the correlated *d* electrons of Cu by means of a mean-field-type Hubbard model, while all other electrons are handled by standard LDA. It leads to an antiferromagnetic state for the undoped materials and also yields reasonable Cu(2) EFGs (Blaha *et al.*, 2002).

6. Structure refinements

All data sets and models presented in this paper are summarized in Table 2. Refinements were started assuming neutral atoms as procrystal (data set ESF/IAM). General

Table 3
Atom positions z (fractional coordinates) and anisotropic thermal displacement factors (ADP) U^{ii} [10^5 Å^2], (C) = constrained to another parameter.

		ESFHO/IAM	ESF/IAM	ESF/HFW	ND
Y	U^{11}	452 (3)	443 (2)	450 (2)	570 (40)
	U^{22}	452 (3)	440 (2)	453 (2)	570 (C)
	U^{33}	561 (3)	558 (2)	557 (2)	500 (30)
Ba	z	0.18381 (1)	0.18381 (1)	0.18381 (1)	0.18369 (9)
	U^{11}	697 (2)	691 (1)	694 (1)	720 (30)
	U^{22}	573 (2)	563 (1)	576 (1)	720 (C)
	U^{33}	722 (2)	716 (1)	720 (1)	650 (30)
Cu(1)	U^{11}	712 (4)	718 (3)	710 (3)	750 (30)
	U^{22}	495 (3)	493 (3)	506 (3)	750 (C)
	U^{33}	502 (4)	489 (3)	512 (3)	520 (30)
Cu(2)	z	0.35489 (1)	0.35489 (1)	0.35487 (1)	0.35484 (5)
	U^{11}	378 (3)	362 (2)	386 (3)	450 (15)
	U^{22}	367 (3)	351 (2)	384 (3)	450 (C)
	U^{33}	802 (3)	798 (2)	786 (3)	810 (20)
O(1)	U^{11}	2010 (30)	1984 (29)	1970 (35)	2300 (100)
	U^{22}	614 (16)	580 (18)	674 (37)	750 (60)
	U^{33}	1406 (24)	1459 (26)	1300 (32)	1300 (90)
O(2)	z	0.37855 (5)	0.37860 (4)	0.37857 (3)	0.37826 (3)
	U^{11}	442 (9)	425 (10)	459 (20)	550 (30)
	U^{22}	715 (11)	722 (12)	694 (10)	770 (20)
	U^{33}	1055 (12)	1063 (13)	1030 (18)	970 (20)
O(3)	z	0.37807 (4)	0.37803 (4)	0.37815 (9)	0.37826 (C)
	U^{11}	697 (10)	714 (11)	617 (27)	770 (C)
	U^{22}	471 (10)	451 (11)	545 (33)	550 (C)
	U^{33}	877 (10)	889 (12)	842 (21)	970 (C)
O(4)	z	0.15896 (4)	0.15894 (3)	0.15897 (3)	0.15870 (8)
	U^{11}	1106 (13)	1134 (15)	1089 (11)	1100 (20)
	U^{22}	866 (13)	890 (15)	856 (10)	1100 (C)
	U^{33}	661 (13)	620 (15)	652 (13)	700 (30)
	$R(F)$	0.0061	0.0071	0.0047	
	$R_w(F)$	0.0085	0.0112	0.0062	0.0494
	GoF	1.38	1.85	1.12	

atom position coordinates z of the atoms Cu(2), O(2), O(3) and O(4) and the anisotropic displacement parameters (ADP) of all atoms were refined independently, *i.e.* no constraints were applied. In addition, an anisotropic extinction model according to the Becker–Coppens formalism (Becker & Coppens, 1974) was used, consisting of two extinction parameters parallel and perpendicular to the flat surface, respectively. First tests showed that the extinction perpendicular to the surface was insignificantly small. Thus, it was neglected in all following refinements. The extinction coefficient parallel to the surface was found to be small, yielding ∼4% extinction for the strongest reflections. No significant differences were found assuming either Lorentzian or Gaussian shapes of the mosaic distribution. All refinements were performed using *VALRAY* (Stewart *et al.*, 2000).

The ADP were checked by refinements using only high-order reflections. We extracted 553 high-order reflections in the range $0.8 < \sin\Theta/\lambda < 1.05$ Å^{-1} for these comparisons. As shown in Table 3, in general there are good agreements between the refined ADP of the high-order structure factors (ESFHO/IAM; column 3) and those of the complete data set (column 4).

It is well known that ADP can correlate with the multipole parameters, especially if the multipole model does not properly describe the experimental density, *e.g.* Stevens & Coppens

(1975), Rees (1978), Kirfel *et al.* (1979). As an example, Table 3 presents the ADP after multipole refinements using Hartree–Fock wavefunctions (column 5). Generally, good agreements were found compared to ESF/IAM and ESFHO/IAM. Exceptions occurred for U^{22} and U^{33} of O(1) and U^{11} and U^{22} of O(3), which show not only differences of about 10% but also considerably larger standard deviations. Inspection of the correlation matrix, however, indicated no significant correlations with other refinement parameters.

Additionally, earlier results of a neutron diffraction experiment presented by Casalta *et al.* (1996) are shown in Table 3, column 6, for comparison purposes. The neutron data have been measured on a twinned crystal of YBa$_2$Cu$_3$O$_{6.96}$ at $\lambda = 1.047$ Å, yielding 375 unique reflections up to $\sin\Theta/\lambda = 0.74$ Å^{-1}. Qualitatively, the X-ray and neutron results agree. Quantitative differences, however, may be ascribed to the fact that the neutron diffraction sample was not monodomain.

An examination of the ADP also reveals some details about the coordination and bonding of the atoms. U^{11} and U^{22} of Y are nearly identical, although not constrained to each other, and they differ from U^{33}. In contrast to the ND results, U^{33} was found to be larger than U^{11} and U^{22}. U^{11} and U^{22} of Ba, however, differ by ∼20%, which reflects the presence of oxygen on the O(1) position at 0,0.5,0 and the vacancy of the O(5) position at 0.5,0,0, respectively. For Cu(2), U^{11} and U^{22} agree well, whereas U^{33} is approximately twice as large, indicating differences between the Cu(2)—O(2) and Cu(2)—O(3) bonds in the superconducting plane on the one hand and the Cu(2)—O(4) bond perpendicular to the plane on the other hand. In contrast, Cu(1) is planar coordinated by O(1) and O(4), which is expressed by the agreement between U^{22} and U^{33} of Cu(1), whereas U^{11}, which is related to the empty O(5) site, differs. In agreement with Casalta *et al.* (1996) and earlier results of an X-ray study by Sullivan *et al.* (1993) on a detwinned crystal of YBa$_2$Cu$_3$O$_{6.877}$, the parameters U^{11} of O(2) and U^{22} of O(3) on the one hand and U^{22} of O(2) and U^{11} of O(3) on the other hand are approximately of the same magnitude. Interestingly, U^{33} of O(2) appears to be about 20% larger than U^{33} of O(3), which might be ascribed to the presence of oxygen on the O(1) site and the vacancy on the O(5) position.

The high-order data were additionally used to check for the existence of anharmonic thermal motions. Using the cumulant expansion (Kendal & Stuart, 1958; Johnson, 1969) in *VALRAY*, the site-symmetry-compatible displacement parameters of third and fourth order were refined, but they turned out to be either very small or even insignificant. Nevertheless, a further test was carried out by applying these small anharmonic thermal motion parameters as fixed values in the model. Compared to refinements using only the harmonic vibration model, no significant improvements of the fits were found. Thus, the third- and fourth-order cumulants were omitted in the following refinements.
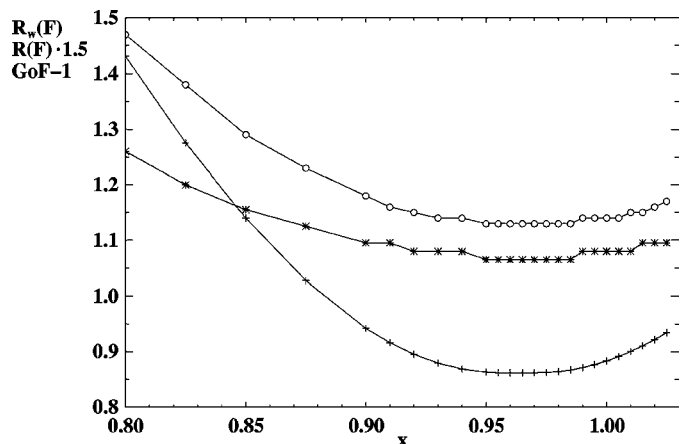
According to the crystal growth procedure, our sample should be fully oxidized, which corresponds to 6.98 oxygen atoms in the chemical formula and 293.84 electrons in the unit cell. In order to check this assumption, refinements were

performed using start parameters for different contents of oxygen in the structure. Since the occupation of a given site cannot be refined in *VALRAY*, the tests were carried out by varying the occupation number of the O(1) site prior to the refinements. The change of the total number of electrons in the unit cell was appropriately compensated for by the scale factor. Fig. 2 shows agreement factors and goodness of fit (GoF) of these tests and indicates that the best fit results by assuming an occupancy of the O(1) site of ∼0.97, indicating that the stoichiometry of the sample was in fact very close to the assumed $YBa_2Cu_3O_{6.98}$. Further refinements were carried out assuming partial occupancy of the O(5) site. All these tests revealed significant degradation of the fits, *i.e.* no significant hints for oxygen on the O(5) site were found.

In order to account for the aspherical parts of the valence density, the IAM was extended by the generalized-structure-factor (GSF) model (Stewart, 1969). Multipoles up to the order $\ell = 4$ were applied. The radial distribution of the core electrons was described by expansions of neutral atom Hartree–Fock wavefunctions (Clementi, 1965) using the bases of Clementi & Roetti (1974). The expansions for Y and Ba were taken from Koga *et al.* (1995) and Thakkar (2001). Valence monopoles ($\ell = 0$) were always modelled using single exponential functions (EXP)

$$R_\ell(r) \propto \alpha_\ell r^{n(\ell)} \exp[-\alpha_\ell r], \qquad (3)$$
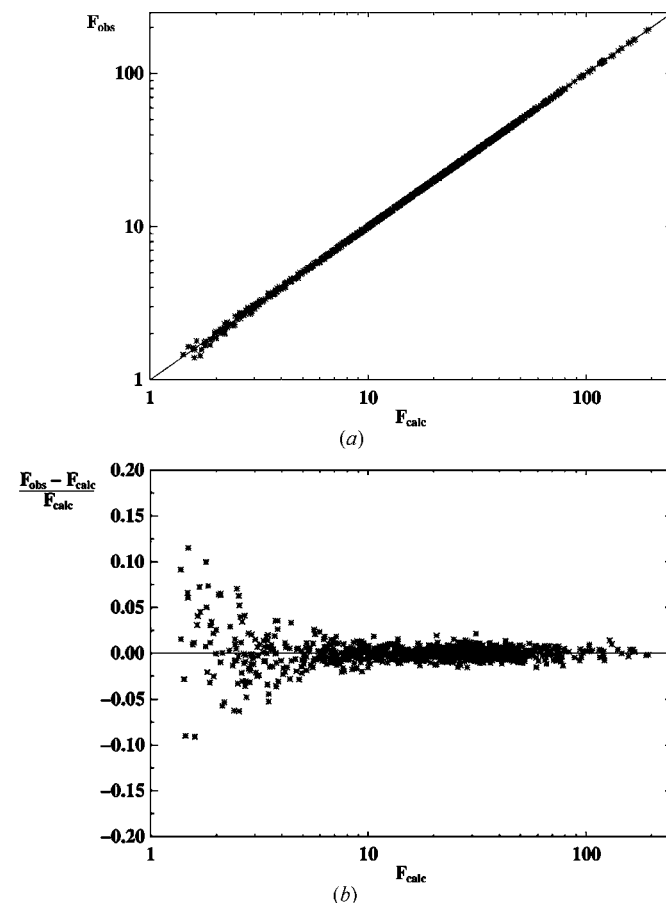
which are also valid for higher-order multipoles ($\ell > 0$). α_ℓ is the radial refinement parameter and $n(\ell)$ is an adjustable integer obeying $n \geq \ell$. The combination of HFW for the core and EXP for the valence electrons was used for two reasons. First, the separation of the analytical functions into core and valence parts is not unique and, therefore, somewhat arbitrary, and, second, a higher flexibility in modelling the charge transfer was achieved by using EXP for the valence electrons (compare LSb). Multipoles of order $\ell > 0$ were refined using either HFW or EXP functions (refinements ESF/HFW and ESF/EXP, Table 2), where in the HFW case the radial refinement was performed using a refinement parameter κ'_ℓ,

which stands for the contraction and expansion of the multipole (Hansen & Coppens, 1978). For each single atom, the radial refinement parameters of multipoles $\ell > 0$ were constrained to a single value.

Refinements were carried out using a new version of the program package *VALRAY* (Stewart *et al.*, 2000; Flensburg & Madsen, 2000), which was extended in order to process wavefunctions of heavy elements, *i.e.* Ba (Flensburg, 2000). The refinement strategy was based on the 'block mode', *i.e.* different types of variables like crystallographic standard parameters or multipole populations were pooled in blocks and refined in alternating cycles in order to achieve convergence of the flexible models. Multipoles up to hexadecapoles ($\ell = 4$) were applied. Octopole and hexadecapole populations turned out to be insignificant, *i.e.* smaller than their standard deviations, in the cases of O(1) to O(3). Further tests using multipoles up to $\ell = 7$ also failed, *i.e.* either the refinements diverged or the populations were insignificant. Each refinement was finished by a final full matrix cycle. A refinement is considered as converged as soon as the relative change of the least-squares deviance is smaller than a certain criterion of convergence. In *VALRAY*, this criterion c is defined as (Stewart *et al.*, 2000)

(a)

Figure 2
Weighted R factor $R_w(F)$ (○), R factor $R(F) \times 1.5$ (∗) and goodness of fit (GoF) − 1 (+) after IAM refinements plotted against occupation x of O(1) site.

(b)

Figure 3
(a) F_{obs} *versus* F_{calc} and (b) relative deviations of structure factors after the multipole refinement ESF/HFW.

$$c = |\mathbf{g}^{\dagger}\mathbf{d}|/\varepsilon(\mathbf{P}), \tag{4}$$

where $\varepsilon(\mathbf{P})$ is the mean square error function at point $\mathbf{P}$ in the n-dimensional space to be minimized, $\mathbf{d}$ is a vector describing a move from point $\mathbf{P}$ to change ε and $\mathbf{g}$ is the gradient of ε. In order to allow subsequent variance analyses and error map calculations, c was set to 10^{-8}.

The multipole analyses were started by a monopole refinement. The model was gradually expanded by including multipoles of Cu and O and finally also multipoles of Y and Ba. Each expansion of the model was checked by application of Hamilton's significance test (Hamilton, 1969). According to these tests, each expansion yielded significant refinement improvements at a confidence level of 99.995. This holds for the application of Y and Ba multipoles as well. Second derivatives were included in the least-squares matrix in order to check if the true refinement minimum was reached. No significant parameter changes were observed comparing refinement results either using or omitting the second derivatives. Additionally, different refinement strategies were tested, *e.g.* refining the multipoles $\ell > 0$ before the monopole

Figure 4
Difference density plots ($\rho_{tot} - \rho_{procrystal}$) of (100) planes ($x = 0$). (*a*) LAPW calculation and (*b*) experimental density (κ' of O atoms constrained, see text). Contour line distance 0.1 e Å^{-3}; cut-off at 1 e Å^{-3}; centre at fractional coordinates $0,0.5,0.2$; positive contours solid; negative broken; zero contour dotted.

parameters. All strategies yielded identical results and variations of the population coefficients and radial parameters, which were much less than the standard deviations.

Special attention was also paid to the anomalous-dispersion corrections f' and f''. Although anomalous dispersion is generally small at 100 keV, which is far from most of the absorption edges, it cannot be completely neglected because the dispersion corrections strongly influence the results of valence monopole population refinements, and thus the charge transfer results. Unfortunately, both theoretical and experimental literature data of 100 keV anomalous-dispersion factors scatter considerably, *e.g.* $f'(\mathrm{Ba})$ in the range -0.2 to 0.5 e atom^{-1}. Therefore, we decided to perform extensive tests by varying the f' and f'' prior to the refinements and inspecting the results with respect to both the refinement quality (agreement factors, GoF) and the 'chemical reasonability', *i.e.* refinements yielding O^{3-}, O^{+}, Y^{-}, Ba^{-} *etc.* were rejected.

According to these tests, reasonable $f'(\mathrm{Y})$ were found in the range 0.1–0.3 e atom^{-1} and $f'(\mathrm{Ba})$ in the range 0.2–0.4 e atom^{-1}, which agree very well with the factors presented by Chandler (1995) (Table 1). Variations of $f'(\mathrm{Cu})$ and $f'(\mathrm{O})$ yielded no significant trends. The same holds for variations of f'' of all atoms. Accordingly, the anomalous-dispersion corrections of Chandler (1995) were applied for all atoms in the following analyses.
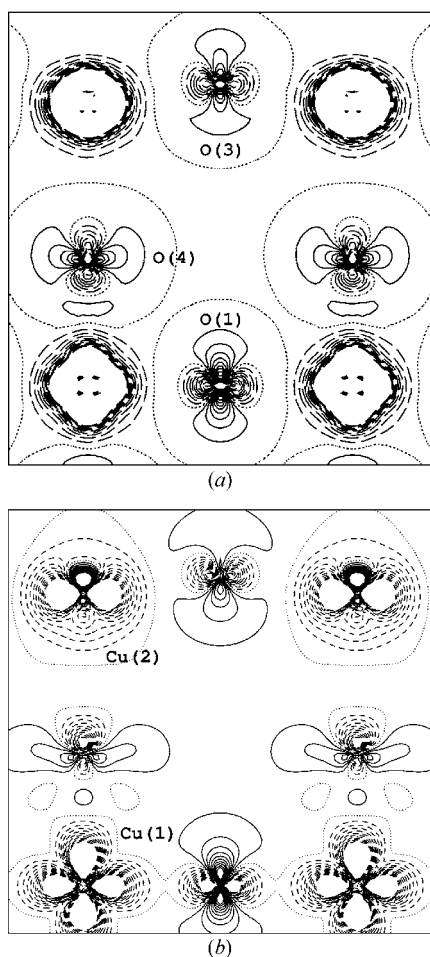
Fig. 3 shows that the experimental structure factors were well refined using the multipole model, *i.e.* appreciable deviations between observed and model structure factors were only found below 3 electrons.

Theoretical structure factors were derived from the LAPW calculations for $T = 0$ K up to the same resolution as the experimental data set. Uniform weights were given to the theoretical data and the same refinement models used as those applied to the experimental data with three exceptions: no ADP, no anomalous-dispersion corrections and no extinction model were included. The TSF were refined to $R(F) = 0.0023$, $R_w(F) = 0.0023$, GoF = 0.59.[2]

7. Charge-density maps

Comparisons between theoretical and experimental charge-density results are often difficult because the results are biased by the models used to calculate the theoretical data and to fit the experimental data. Thus, in the maps shown below, mainly charge densities from theoretical and experimental structure-factor refinements are compared where in both cases the same refinement model was used. On the other hand, a direct comparison between the experimental and the LAPW density gives an overview of main similarities or differences, as shown in Fig. 4. Here, in both cases, the charge density of the procrystal is subtracted from the total density and a good overall agreement is found. In both cases on average, a negative density around Cu and a positive density around O is found. Whereas the density features around the O atoms are

---

[2] A summary of all numerical results (multipole populations and radial parameters) is presented by Lippmann (2002).
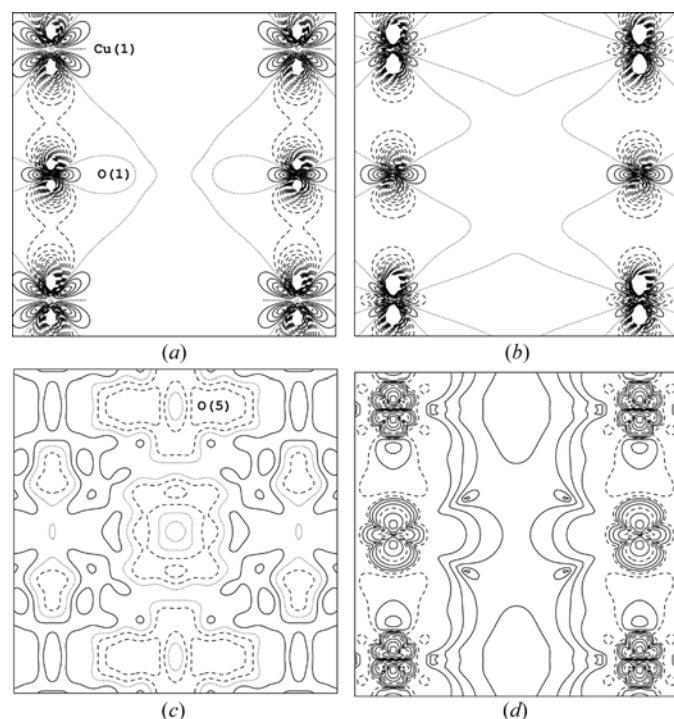
Table 4
Radial parameters of the refined multipoles.

Units are: κ' dimensionless; α a.u.; (c) oxygen parameters constrained to each other.

Multipole model Data set	HFW (κ')			EXP (α)		
	ESF	TSF	CSF	ESF	TSF	CSF
Y	0.38 (3)		0.39 (3)	5.13 (71)		5.30 (82)
Ba	0.82 (2)	1.28 (16)	0.81 (2)	8.68 (53)	1.17 (17)	8.59 (52)
Cu(1)	0.69 (4)	1.02 (6)	0.70 (4)	5.99 (24)	8.07 (37)	5.98 (24)
Cu(2)	0.99 (6)	0.92 (5)	0.99 (6)	7.48 (28)	7.42 (32)	7.46 (28)
O(1)	1.34 (15)	1.24 (10)	1.23 (13)	5.11 (70)	5.33 (34)	3.58 (23)
O(2)	0.93 (11)	1.35 (11)	(c)	2.57 (54)	5.76 (37)	(c)
O(3)	1.84 (16)	1.28 (10)	(c)	6.89 (63)	5.60 (34)	(c)
O(4)	0.83 (14)	1.71 (15)	(c)	3.13 (25)	7.16 (56)	(c)

rather similar comparing experimental and theoretical maps, differences in the anisotropy of the charge density at the Cu atom sites are more pronounced. The reason was found in a difference of the spherical contribution (valence monopole), which is superimposed on the deformation contribution. According to the LAPW calculation, the Cu monopoles are more contracted. Thus, they dominate the Cu density in the theory map.

Static deformation density maps of various planes were calculated from both theoretical and experimental structure factors (F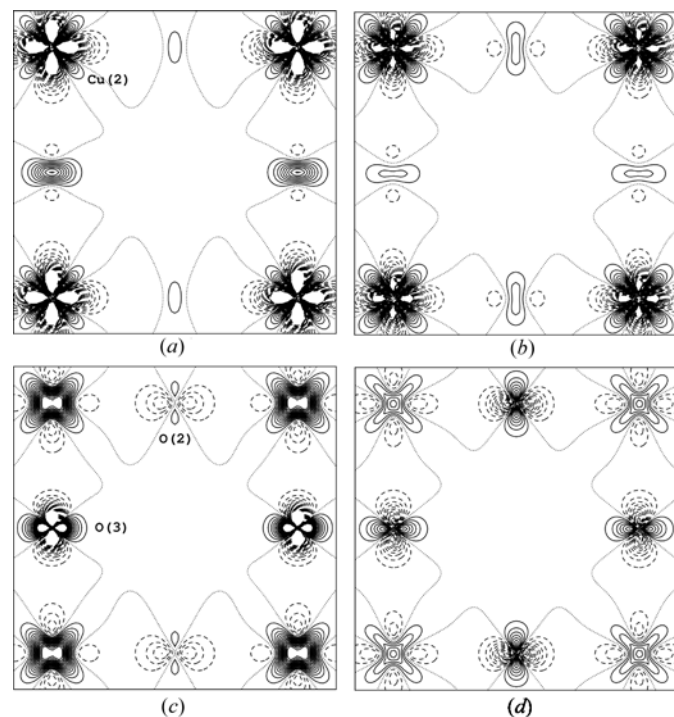igs. 5–8). Additionally, the residual density and an error map of the experimental results are shown in Fig. 5. The most striking common features of both theoretical and experimental maps are the charge-depletion regions between the Cu and O atoms. In general, the residual densities of the experimental results indicate a good agreement between the multipole model and the observed structure factors and show no additional unmodelled charge accumulation in the interatomic regions.

In a detailed comparison of the copper deformations, the agreement between the Cu(1) atoms (Figs. 5 and 7) is excellent, although the theoretical density is slightly more contracted (Table 4). Strong charge depletion is found in the directions towards O(1) and O(4), whereas only small deformation density is found towards the empty O(5) site.

The experimental deformation features of Cu(2) in the (001) plane qualitatively match very well the theoretical contours (Figs. 6a,b). Charge depletion regions were found along the bond paths of Cu(2) and the neighbouring O atoms O(2) and O(3). Perpendicular to the (001) plane, however, differences were found (Figs. 7 and 8). The experimental deformation density reveals a significant dipole contribution, which gives a hint for a lone pair pointing away from O(4). In the theoretical results, the dipole and octopole contributions of Cu(2) were nearly insignificant. Thus, the experimental deformation density maps show small features and a slightly depleted region between Cu(2) and O(4), and a charge
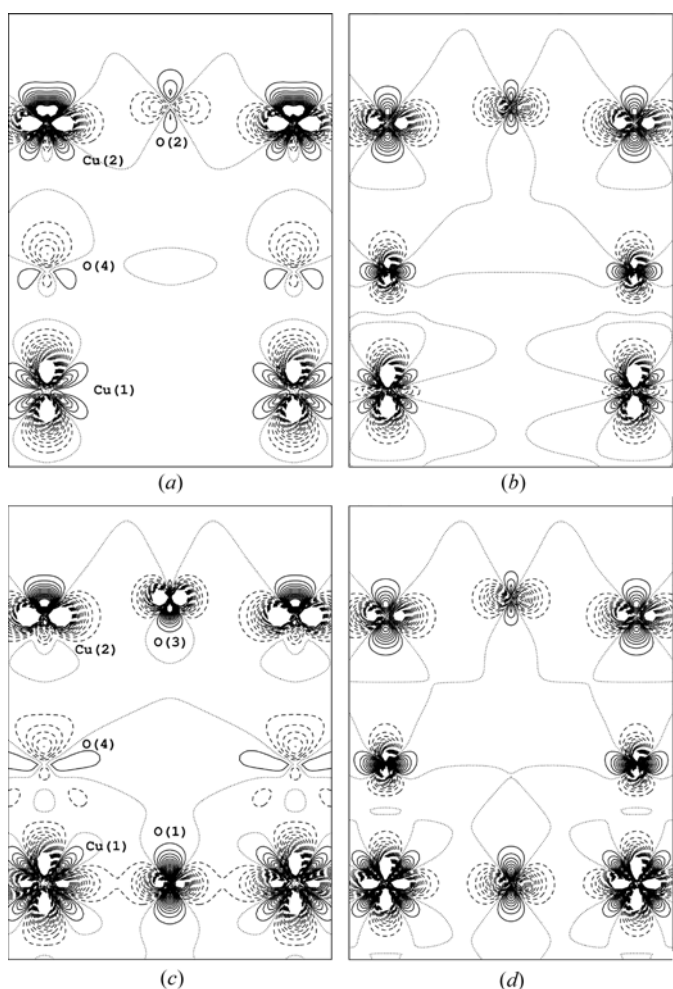

Figure 5
Charge-density plots of (001) planes ($z = 0$). 5×5 Å, centre at fractional coordinates 0.5, 0.5, 0. (a) Static deformation density from experimental data (ESF/HFW, monopoles omitted). (b) Static deformation density from theoretical data (TSF/HFW). (c) Residual density from experimental data refinement. (d) Error map of the total charge density from experimental data. (a), (b), (c) Positive contours solid, negative broken, zero contour dotted, contour line distance 0.1 e Å^{-3}, cut-off at 1.5 e Å^{-3}. (d) Contour lines on a geometrical scale, starting at 0.0001 e Å^{-3}, line n at 0.0001×2^n. Lines at 0.006 and 0.1 e Å^{-3} are dashed.

Figure 6
Charge-density plots of (001) planes (a, b: $z = 0.355$; c, d: $z = 0.378$); (a), (c): ESF/HFW; (b), (d): TSF/HFW. Plot parameters according to Figs. 5(a), (b).
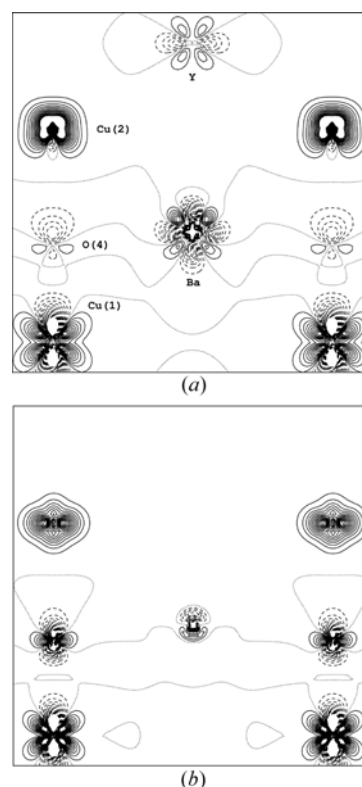
research papers

accumulation on the opposite site of the Cu atom. In contrast, the theoretical map indicates small density accumulations on both sides of Cu(2) along the c axis, *i.e.* the only case where a small charge accumulation along a Cu—O bond was found in the deformation density.

As was already mentioned, calculations based on LDA cannot obtain an insulating antiferromagnetic ground state in the undoped parent compounds nor describe the EFG at the Cu(2) site properly (Schwarz *et al.*, 1990). In particular, the latter fact points out that the theoretical charge density cannot be completely correct since LDA cannot fully take into account the strong onsite correlations of the Cu d shell. Thus, we have performed LDA+U calculations and such calculations are able to reproduce both the AFM insulating state of $YBa_2Cu_3O_6$ and the correct EFG in high-T_c superconductors (Blaha *et al.*, 2002). Here we want to check whether the density obtained from such a LDA+U calculation is in better agreement with experiment and in particular whether it has a significant dipole contribution. In Fig. 9, we plot the difference between the LDA+U and LDA density in the (100) plane. We

do find a significant difference at the Cu(2) site, however, no significant dipole contribution is observed, so that also the LDA+U calculations cannot verify the experimentally observed asymmetry. The changes in the charge density can be interpreted as a redistribution of charge density from $d_{x^2-y^2}$ orbitals into d_{z^2} states, since the latter have weaker anti-bonding character owing to the larger Cu(2)—O(4) distance compared to the inplane Cu—O distances. The charge density around all other atoms is nearly unchanged.

Figure 8
Charge-density plots of (110) planes. 7×7 Å, centre at fractional coordinates $0.5, 0.5, 0.25$. Plot parameters according to Figs. 5(a), (b).

Figure 7
Charge-density plots of (010) planes ($y = 0$) (a, b) and (100) planes ($x = 0$) (c, d). 5×7 Å, centre at fractional coordinates $0.5, 0, 0.2$ and $0, 0.5, 0.2$, respectively; (a), (c) ESF/HFW; (b), (d) TSF/HFW. Plot parameters according to Figs. 5(a), (b).
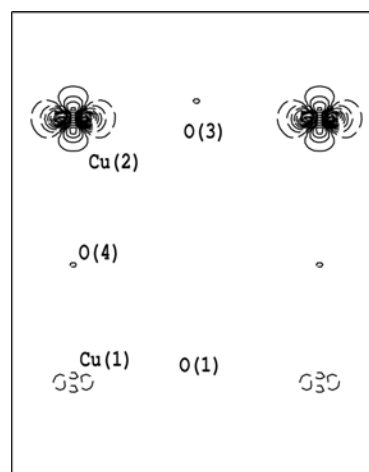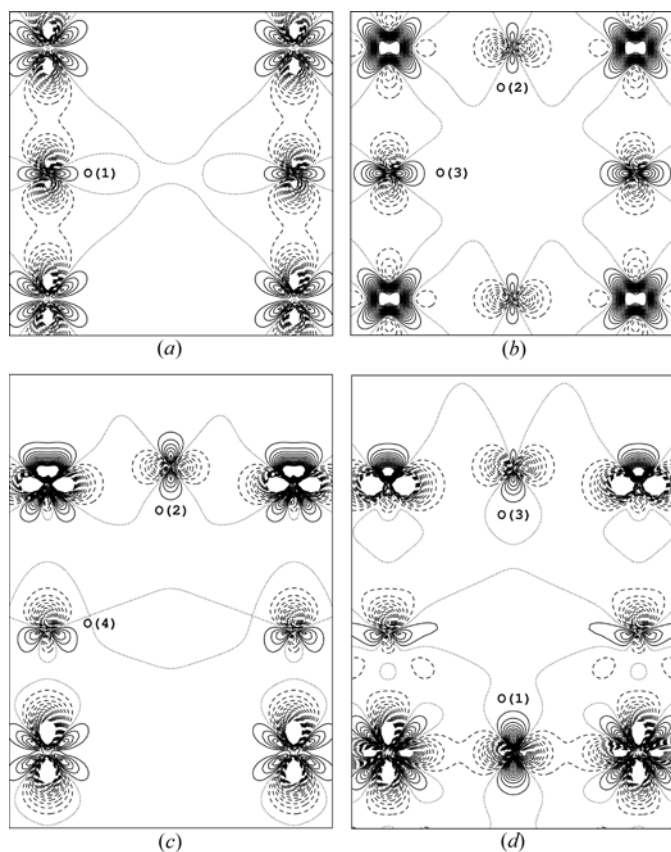

Figure 9
Difference charge density in the (100) plane ($x = 0$) between theoretical LDA+U and standard LDA calculations. Positive contours solid, negative broken, contour line distance 0.1 e Å^{-3}, starting at 0.05 e Å^{-3}.

When the oxygen charge deformations between theory and experiment are compared, two significant differences become obvious. The first is based on the shapes of the oxygen deformation densities, *i.e.* the contraction and expansion of the multipoles. According to the LAPW data, the radial deformation-density distributions are approximately identical for all O atoms, *i.e.* the O atoms look very similar. The experimental maps reveal considerable differences between the contracted density of O(3) on the one hand and the expanded densities of O(2) and O(4) on the other (Figs. 6c,d and 7). Only the experimental deformation density of O(1) is comparable to the theoretical result. Table 4 indicates that the experimental deformation densities of O(2) and O(4) on the one hand and O(3) on the other hand differ by the radial parameters κ'. It is well known that in multipole refinements the radial parameters sometimes show a tendency to adopt unreasonably small or large values either because of correlations with other refinement parameters or due to insufficient resolution, *i.e.* the number of observed reflections is too small for a proper determination of the radial parameters. Thus, it cannot be excluded that one of these reasons is responsible for observing different shapes of the oxygen valence densities in the experimental results. In fact, the variance analysis revealed enhanced correlations of about 90% between the radial

parameter κ' of O(3) and the O(3) ADP, which might be the reason for the strong contraction of the O(3) density. Thus, further refinements were carried out, where all radial parameters of all O atoms were constrained to each other (CSF/HFW and CSF/EXP). These constraints only had a small influence on the results of the multipole population coefficients of the O atoms and no significant effect on the refinement parameters of the other atoms compared with the unconstrained refinement. The resulting κ' of 1.23 and the radial density distribution (Fig. 10), however, were found to be in better agreement with the LAPW density (Figs. 5b, 6d, 7d and Table 4).

A second principal difference between theoretical and experimental oxygen deformation densities is the polarization of the O(3) and O(4) deformations along the c_0 axis in the experimental maps, whereas theory indicates no polarization of O(3) and small polarization of O(4). This result was obtained independently of using either CSF or ESF refinements (*e.g.* Figs. 7 and 10). The density of O(3) is depleted towards the above-lying O(3) and accumulated in the void between O(3) and O(1), whereas the neighbouring Cu(2) atoms reveal reverse polarizations, *i.e.* depletion towards O(4) and accumulations in the voids between two adjacent coppers. From this observation, one may conclude that the density tends to accumulate in the structural voids of $YBa_2Cu_3O_{6.98}$. In contrast to O(3), the experimental O(2) density is not polarized. Thus, it cannot be excluded that the presence of O(1) and the absence of oxygen on the O(5) site also has an influence on the charge deformation features in the super-

Figure 10
Static deformation density plots of experimental density from refinements using the κ' constraints for the O atoms (see text). (a) (001) plane ($z = 0$). (b) (001) plane ($z = 0.378$). (c) (010) plane ($y = 0$). (d) (100) plane ($x = 0$).
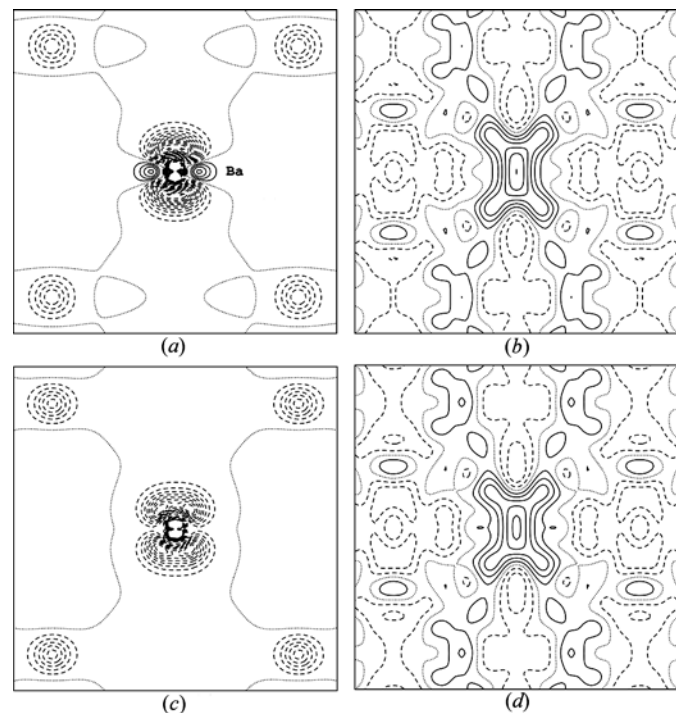
Figure 11
Charge-density plots of (001) planes ($z = 0.184$). Static deformation density omitting (a) and including (c) anharmonic displacement parameters of Ba. (b), (d) Corresponding residual densities.

conducting O(2)—Cu(2)—O(3) plane. The polarization of the O(4) density, however, is probably correlated with both the differences between the Cu(1)—O(4) and the Cu(2)—O(4) bond lengths and with the presence of the Ba ion.

The EFG at the different atomic sites can be measured accurately by *e.g.* NQR spectroscopy and was experimentally found to be much larger for O(1) (17.3×10^{21} V m^{-2}) than for the three other O sites, which have quite similar EFGs (10.5, 10.2 and 11.6×10^{21} V m^{-2}), with O(4) about 10% larger than O(2,3) (Schwarz *et al.*, 1990). Since the EFG can be obtained by an integral over the $1/r^3$ weighted non-spherical density, it is clearly connected to the non-spherical charge distribution. This requires that the non-spherical density around O(2) and O(3) must be quite similar, whereas it ought to be much more pronounced around O(1). The present experimental charge density does not reproduce these results (Fig. 10), but the theoretical density does and it also reproduces the measured EFGs quite accurately (Schwarz *et al.*, 1990).

As illustrated in Fig. 8, there are also differences between the experimental and theoretical deformations of the heavy ions Y and Ba. The LAPW data reveals no deformation of Y and very small deformation near Ba, whereas the experiment indicates considerable deformation density here. The shapes of the lobes in the residual density maps (Fig. 11*b*), however, closely resemble those found in the cases of anharmonicity (Buttner & Maslen, 1992; Sasaki *et al.*, 1992). Thus, a further test was performed, where anharmonic thermal motion parameters for Ba were refined together with multipole parameters, although strong correlations were present. No significant improvement was found and the residual density at the Ba site was only marginally reduced (Fig. 11*d*). The only difference was that the octopole contribution Y_{32+} was now replaced by the higher cumulants c_{113} and c_{223}. As a consequence and taking into account that residual density at the Ba site amounts to 0.5 e Å^{-3}, it is evident that the modelling of the Ba density is not perfect and needs further improvements.

According to analyses of the partial densities of states, which are not presented here, it is known that in Ba the *s* and *p* orbitals are lying above the Fermi level and are therefore mainly unoccupied. Thus, from a theoretical point of view, we find more or less a Ba^{2+} ion, *i.e.* almost all valence electrons are lost and the density must be nearly spherical (if one accepts that the shallow Ba 5*p* core states still have a spherical density). On the other hand, Y retains more or less it's 4*d* electron (but loses both 5*s* electrons) and this *d* charge could in principle lead to significant anisotropy. Nevertheless, in theory the 4*d* charge is quite spherical (all *d* orbitals have similar occupation) indicating that there are no direct covalent interactions present.

In general, for both Y and Ba, the locations of accumulation and depletion lobes are not correlated with the bond paths of Y—O and Ba—O bonds. Thus, it can be concluded that the interactions between the heavy ions and the Cu—O frame is obviously less than the interaction between Cu and O themselves. A quantitative examination of this observation is attempted in critical point analysis (see below).

Concerning the situation on the 'empty' O(5) site, according to the residual density plot (Fig. 5), there is no significant charge density here, which is in good agreement with the test results of the variation of the occupancy of the O(5) site presented above.

8. Topological analysis

A quantitative investigation of the bonding in YBa$_2$Cu$_3$O$_{6.98}$ was performed by means of a topological analysis according to the quantum theory of atoms in molecules (AIM) (Bader, 1990, 1998). The analysis was separated into two parts: an investigation of the critical points, where the gradient of the charge density $\nabla\rho(\mathbf{r})$ vanishes, and the calculation of Laplacian maps $L(\mathbf{r}) = \nabla^2\rho(\mathbf{r})$, *i.e.* the trace of the diagonalized Hessian matrix, which is the sum of the principal curvatures λ_1, λ_2 and λ_3. The bond critical points (b.c.p.), where the principal curvature parallel to the bond is positive and the curvatures perpendicular to the bond are negative, yield useful bonding information because a positive Laplacian and a small charge density at these points indicates closed-shell interaction (ionic bonding), whereas a small or negative value of $\nabla^2\rho(\mathbf{r})$ and relatively large density is a hint for covalent bonding (Bader & Essen, 1984).

The search for critical points was carried out using a narrow three-dimensional grid (0.1 Å grid interval) as starting points and the algorithm implemented in *VALRAY*. After elimination of the duplicates, the search yielded 98 points in the experimental and 118 points in the theoretical density. Both sets obey the Morse equations (Morse & Cairns, 1969; Pendas *et al.*, 1997)

$$
\begin{aligned}
n - b + r - c &= 0 \quad & n \geq 1, \ b \geq 3, \ r \geq 3, \ c \geq 1 \\
13 - 45 + 36 - 4 &= 0 \quad & \text{experiment} \\
13 - 45 + 46 - 14 &= 0 \quad & \text{theory,}
\end{aligned}
\tag{5}
$$

where n are local maxima, b are bond points, r are ring points and c are local minima. Differences between experiment and theory results were caused by some additional ring points (r.c.p.) and minima in the theoretical density close to the special positions at fractional coordinates 0,0,0.5 and 0.5,0,0, respectively. Since the second derivatives of all these points were close to zero, they might be artefacts of the calculation. Additionally, r.c.p. and minima were found near the midpoint of the Ba–Ba connecting lines. A search for corresponding points in the experimental density failed.

The maxima were exclusively located at the 13 nuclei in the unit cell, *i.e.* no non-nuclear maximum was found. The densities at the local minima and ring points were checked for positivity. The absolute charge-density minimum was 0.06 e Å^{-3}, thus no unphysical 'negative' density was found.

With the symmetry relations taken into consideration, 14 unique b.c.p. were found in both the theoretical and experimental densities.[3] Table 5 lists the b.c.p. from synchrotron data and theory, where for the latter both the directly calculated

---

[3] A list of all critical points is available in Lippmann (2002).

Table 5
(3, −1) bond critical points in $YBa_2Cu_3O_{6.98}$ from experimental (upper rows), theoretical – *via* structure-factor fit (middle rows) and theoretical – direct calculation (lower rows) charge densities.

x, y, z: fractional coordinates; ρ: charge density [e Å^{-3}]; $\nabla^2\rho$: Laplacian [e Å^{-5}]; $|\lambda_1|/\lambda_3$: ratio of principal curvatures; α: angle atom 1– b.c.p.–atom 2.

Atoms	x	y	z	ρ	$\nabla^2\rho$	$|\lambda_1|/\lambda_3$	α (°)
Cu(1), O(1)	0.0	0.2413 (8)	0.0	0.506 (11)	12.46 (30)	0.082 (12)	180
	0.0	0.2505 (5)	0.0	0.566 (7)	10.17 (6)	0.160 (10)	180
	0.0	0.2474	0.0	0.629	9.51	0.174	
Cu(1), O(4)	0.0	0.0	0.0752 (3)	0.615 (22)	18.12 (57)	0.052 (16)	180
	0.0	0.0	0.0789 (2)	0.755 (10)	13.72 (13)	0.167 (11)	180
	0.0	0.0	0.0784	0.813	11.26	0.198	
Cu(2), O(2)	0.2425 (6)	0.0	0.3689 (7)	0.571 (11)	11.84 (15)	0.137 (10)	177.4
	0.2500 (3)	0.0	0.3672 (2)	0.636 (5)	10.97 (6)	0.171 (5)	179.3
	0.2483	0.0	0.3661	0.659	7.51	0.215	
Cu(2), O(3)	0.0	0.2406 (6)	0.3680 (5)	0.540 (8)	10.75 (10)	0.144 (11)	177.9
	0.0	0.2497 (3)	0.3680 (2)	0.593 (4)	9.84 (5)	0.170 (5)	179.3
	0.0	0.2476	0.3669	0.611	7.34	0.195	
Cu(2), O(4)	0.0	0.0	0.2585 (5)	0.294 (8)	3.07 (9)	0.222 (16)	180
	0.0	0.0	0.2565 (1)	0.307 (1)	3.67 (1)	0.163 (3)	180
	0.0	0.0	0.2574	0.290	3.59	0.175	
Y, O(2)	0.5	0.2448 (13)	0.4367 (8)	0.321 (5)	4.67 (3)	0.153 (5)	176.8
	0.5	0.2385 (2)	0.4353 (1)	0.335 (1)	4.40 (5)	0.157 (1)	179.7
	0.5	0.2421	0.4367	0.320	3.90	0.201	
Y, O(3)	0.2409 (10)	0.5	0.4363 (5)	0.344 (3)	4.94 (1)	0.157 (6)	180
	0.2375 (3)	0.5	0.4362 (1)	0.360 (1)	4.82 (1)	0.159 (1)	179.8
	0.2417	0.5	0.4373	0.348	4.27	0.203	
Ba, O(1)	0.2231 (17)	0.5	0.0866 (5)	0.199 (1)	2.02 (1)	0.149 (3)	176.3
	0.2214 (7)	0.5	0.0855 (2)	0.167 (1)	1.97 (1)	0.140 (2)	177.5
	0.2340	0.5	0.0842	0.161	1.77	0.170	
Ba,O(2)	0.5	0.2367(24)	0.2886(7)	0.164 (1)	1.69 (2)	0.133 (3)	178.5
	0.5	0.2357 (3)	0.2893 (1)	0.161 (1)	1.64 (1)	0.131 (1)	178.1
	0.5	0.2326	0.2888	0.131	1.53	0.144	
Ba, O(3)	0.2389 (7)	0.5	0.2887 (2)	0.168 (1)	1.68 (1)	0.136 (1)	177.9
	0.2357 (4)	0.5	0.2901 (1)	0.163 (1)	1.66 (1)	0.133 (1)	178.2
	0.2317	0.5	0.2896	0.134	1.55	0.148	
Ba, O(4)	0.2127 (7)	0.2442 (8)	0.1697 (5)	0.236 (1)	2.51 (1)	0.189 (3)	173.8
	0.2257 (2)	0.2274 (2)	0.1718 (1)	0.227 (1)	2.54 (1)	0.157 (1)	178.0
	0.2303	0.2281	0.1707	0.216	2.29	0.179	
O(2), O(2)	0.5	0.0	0.5	0.182 (6)	1.25 (4)	0.180 (30)	180
	0.5	0.0	0.5	0.170 (1)	1.12 (1)	0.186 (1)	180
	0.5	0.0	0.5	0.120	1.34	0.170	
O(3), O(3)	0.0	0.5	0.5	0.183 (1)	1.17 (1)	0.185 (1)	180
	0.0	0.5	0.5	0.182 (1)	1.20 (1)	0.192 (1)	180
	0.0	0.5	0.5	0.130	1.45	0.176	
Cu(1), Cu(1)	0.5	0.0	0.0	0.063 (1)	0.21 (1)	0.013 (3)	180
	0.5	0.0	0.0	0.061 (1)	0.18 (1)	0.023 (5)	180
	0.5	0.0	0.0	0.035	0.18	0.112	

b.c.p.s and the one *via* the *VALRAY* fit are given. The table shows that the b.c.p. properties directly taken from the LAPW data and those from the refined theoretical charge density do not completely match. This indicates that the density far from the nuclei is considerably biased by the model and this should be born in mind for the quantitative interpretation of the results.

The b.c.p. in $YBa_2Cu_3O_{6.98}$ can be divided into three groups, which differ by both absolute sizes of densities and Laplacians: first the copper–oxygen b.c.p., second the Y– and Ba–O b.c.p., and third the b.c.p. found between the O(2), the O(3) and the Cu(1) atoms, respectively.

In the first group, both the densities and Laplacians at the b.c.p. are similar to those found in cuprite (LSb). A detailed examination of these properties revealed additional differences inside the group. For instance, the densities and Laplacians for Cu(1)−O(1), Cu(1)−O(4), Cu(2)−O(2) and Cu(2)−O(3) differ from those at the Cu(2)−O(4) b.c.p., which are considerably smaller. It is interesting to note that the results can be well associated with the bond lengths, which are about 2.3 Å for Cu(2)−O(4) but ∼1.9 Å in the cases of the other Cu−O bonds (Fig. 12).

The densities and Laplacians at the b.c.p. in the Y− and Ba−O bonds are smaller compared with the Cu−O b.c.p. properties. For Y−O, the atom distances are 2.4 Å, the densities are about 0.34 e Å^{-3} and the Laplacians 4.7 e Å^{-5} and, for Ba−O, distances of about 2.9 Å correspond to densities of about 0.18 e Å^{-3} and Laplacians of about 1.8 e Å^{-5}. An exception was found at the Ba−O(4) b.c.p., where the smaller distance of 2.7 Å is reflected by a density of 0.23 e Å^{-3} and a Laplacian of 2.5 e Å^{-5}.
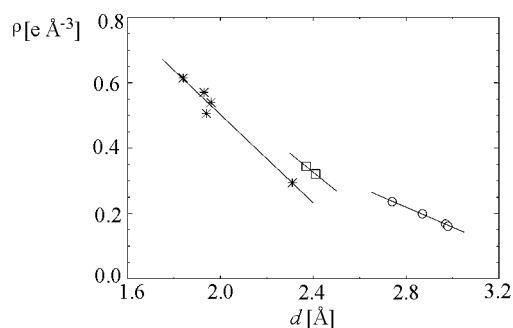
For the first two groups of b.c.p., differences between directly and indirectly calculated theoretical b.c.p. and differences between theory and experiment are small in general.

The positions of the b.c.p. vary within at most 0.02 Å. An exception occurred at the Cu(1)—O(4) b.c.p. Both the densities and Laplacians differ more in this case, *i.e.* the experimental density is smaller than the theoretical result, and the theoretical Laplacian is smaller than the experimental one. Moreover, the directly calculated quantities differ even more from experiment than the fitted ones. The differences of the Laplacians can be primarily ascribed to λ_1 and λ_2, which are -1.05 e Å^{-5} according to the experiment and -3.2 e Å^{-5} according to the LAPW calculation, whereas λ_3 is about 20 e Å^{-5} in both cases. Another interesting result is the b.c.p. between Ba and O, where in most cases the difference between the directly and fitted theoretical b.c.p. is much larger than between theory and experiment, indicating some bias caused by the Ba fit functions.

The last three b.c.p. are located on highly symmetrical sites between O or Cu atoms. Both densities and Laplacians of these b.c.p. are very small and therefore bonding along these paths seems to be improbable here, especially in the case of Cu(1)–Cu(1). Thus, it cannot be excluded that the presence of bond points here is simply an artefact of the long-range exponential functions, which have been used for modelling the valence density. On the other hand, these b.c.p. are also present in the direct theoretical calculation, although again a fairly large difference between the two theoretical b.c.p. are found.

Since, if symmetry relations are absent, the b.c.p. need not be located on the direct connection line between two atoms (Luana *et al.*, 1997), the angles α at the critical points between two atoms, *i.e.* the angles 'atom 1—b.c.p.—atom 2', were additionally calculated and shown in Table 5. Compared to straight bonds (180°), deviations of up to about 6° occur, which are in general more pronounced in the experimental results.

Maps of Laplacians are useful to detect density accumulations in the bonds because the negative Laplacian indicates valence-shell charge concentrations (VSCCs). A detailed analysis of the Laplacians, however, is beyond the scope of this paper and thus we only present an example here. Figs. 13(*a*), (*b*) show Laplacians in the O(1)—Cu(1)—O(4) plane in the usual convention, *i.e.* with $-\nabla^2\rho$ at the top. The maps indicate a twofold symmetry in the oxygen valence shells and charge

concentrations approximately perpendicular to the Cu—O bonds, thus underlining the charge-density results presented above. The maxima of the experimental and theoretical Laplacians at the valence shells of O(1) and O(4) are comparable in height and shape. Figs. 13(*c*), (*d*) show the same Laplacians on a different scale, *i.e.* adjusted to the copper valence shell. Here, the fourfold symmetry becomes obvious and, again, the absolute values of experimental and theoretical Laplacians agree. Finally, maps in Figs. 13(*e*), (*f*) show $+\nabla^2\rho$ at the top. Here, considerable differences between O(1) and O(4) were found. The region surrounding O(1) is approximately homogeneous, whereas the O(4) region is structured and has nearly fourfold symmetry. This result was found both in the theoretical and the experimental maps, although it is much more pronounced for the experimental Laplacian.
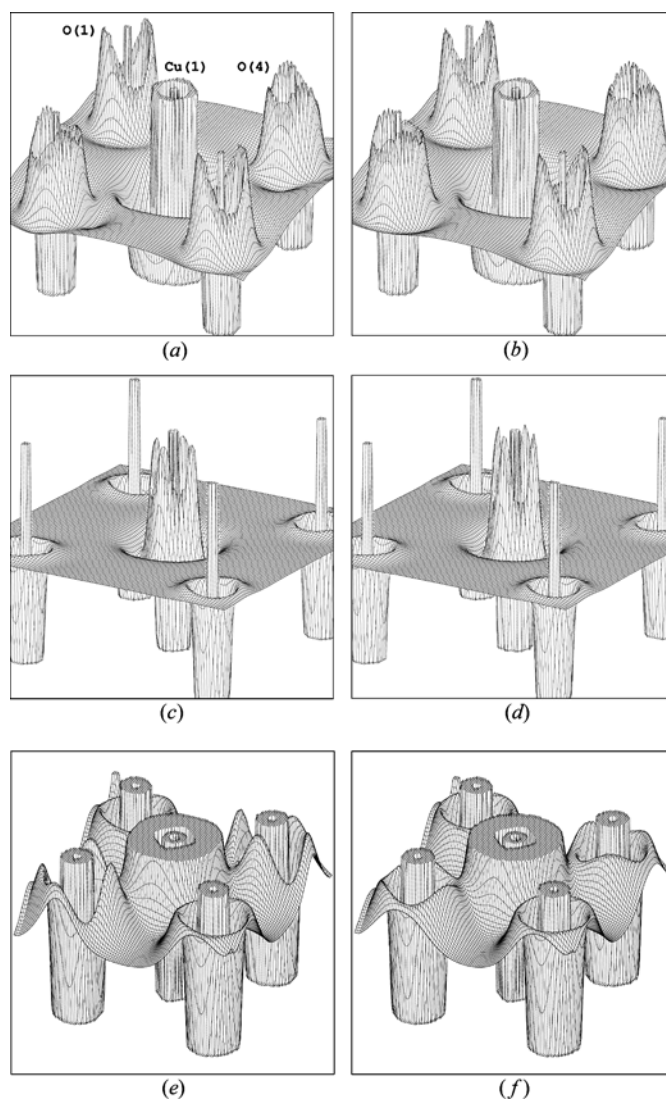
Figure 13
Laplacian maps ($\nabla^2\rho$) calculated from experimental (*a*), (*c*), (*e*) and theoretical (*b*), (*d*), (*f*) charge density. O(1)—Cu(1)—O(4) plane, 4×4 Å, (*a*), (*b*) $-\nabla^2\rho$ to the top, cutoff at -100 e Å^{-5}; (*c*), (*d*) : $-\nabla^2\rho$ to the top, cutoff at -2000 e Å^{-5}; (*e*), (*f*) $+\nabla^2\rho$ to the top, cutoff at 18 e Å^{-5}.

Figure 12
Charge density ρ at the bond critical points *versus* bond distances *d*. Cu—O bonds (asterisks), Y—O bonds (squares) and Ba—O bonds (circles). The figure shows additional regression lines as guides to the eye.

9. Discussion

Up to now, most charge-density analyses have been performed on structures that consist of light first- and second-row elements or transition metals. This limitation can be explained by the increasing amount of core electrons of heavier elements. Stevens & Coppens (1976) proposed the term

$$S = V \Big/ \sum n_{\mathrm{core}}^2 \qquad (6)$$

as a suitability criterion for charge-density analyses, where V is the volume of the unit cell and n_{core} is the number of core electrons. The smaller the value of S, the larger is the problem to separate the contributions of the valence electrons from those of the core electrons, i.e. the difficulties to study the deformation density and the bonding increase. For light-element structures, S typically adopts values from 5 to 0.1 $\mathring{A}^3\,e^{-2}$, but it is only 0.016 $\mathring{A}^3\,e^{-2}$ in the case of $YBa_2Cu_3O_{6.98}$. However, this criterion is no strict rule to allow or reject a charge-density study, but should be regarded as a measure for the increasing difficulty in separating the valence-density information from the core contribution. In fact, the present study shows that, even if heavy elements are present in a crystal structure, it is possible to perform a charge-density study, provided that the method, which is used to measure the data, and the crystal quality are appropriate.

From the b.c.p. properties, i.e. the charge densities, the Laplacians and the $|\lambda_1|/\lambda_3$ ratios at the b.c.p.s, one can interpret the structure as dominated by ionic bonding. However, ionic dominated bonds can also have a partly covalent character, which is for example well known for the Si—O bond, as recently again found in an investigation of stishovite (Kirfel *et al.*, 2001).

Nevertheless, the existence of charge depletion regions between the Cu and O atoms are a clear indication for an additional covalent contribution to the bonding, which is present besides the general ionic contribution. In atoms with more than half-filled shells, a covalent bond is characterized by antibonding orbitals pushed up in energy, making them only occupied up to the Fermi level, while the non-bonding orbitals (pointing into empty space) are fully occupied. Thus, deformation density maps, where the spherical part of the charge density is omitted, show a charge depletion in the bonding direction and an accumulation into empty space. On the other hand, for atoms on the left side of the Periodic Table, the bonding orbitals would be predominantly occupied and a charge accumulation would be present in the deformation density of a covalent bond.

Thus, the deformation density of the copper atoms give strong evidence for unoccupied antibonding $d_{x^2-y^2}$ orbitals along the Cu—O bonds and occupied d_{z^2}, d_{xy}, d_{xz} and d_{yz} orbitals pointing towards the structural voids. As expected, this effect is more pronounced the shorter the respective Cu—O bonds are, since for shorter bonds the bonding–antibonding splitting is expected to be larger leading to even less occupation of the antibonding orbital.

The comparison of the theoretical and experimental results presented in the above sections indicated an overall agreement with respect to the main features of the charge density in $YBa_2Cu_3O_{6.98}$. Nevertheless, there are also some differences and discrepancies, which are worthwhile discussing. For example, the theoretical deformation density maps show a small charge accumulation pointing from Cu(2) towards O(4), which was not found in the experimental density. A further disagreement appears in the O(2)—Cu(2)—O(3) plane, where the experimental oxygen deformation densities of O(2) and O(3) differ, whereas the theoretical densities agree well with each other. Admittedly, the strong contraction of the experimental O(3) density and the expansion of the O(2) density could be fully ascribed to their radial distribution parameters, which are well known to be extremely sensitive to even small inconsistencies in the data, although no indications for such inconsistencies have been found in the data set. On the one hand, it seems physically and chemically unreasonable that the oxygen deformation density is excessively contracted as found in the case of O(3) here. On the other hand, there is also no mandatory reason to favour the constraints of the charge densities of atoms, which are independent from a crystallographic viewpoint. Thus, the results and the charge-density maps shown here should be regarded as border cases, and this is also the reason for the presentation of both constrained and unconstrained densities in this paper. We hope that further experimental studies will provide more details in order to answer this open question.

A further difference between experimental and theoretical densities is the dipole contributions at the Cu(2) and the O sites in the experimental results, which model the polarizations of the deformation densities along the c axis. These are nearly completely absent in the theoretical maps. Such charge polarizations are consistent with the point symmetry of the atoms, but one must also admit the relatively large correlations between the z coordinate of the Cu(2) site and the dipole contribution, which can exceed 0.75. However, one could also argue that the theoretical density needs further improvements because also the theoretical EFG at the Cu(2) site is not correct. LDA+U calculations, which are, however, not fully *ab initio*, can also properly model the EFG at the Cu(2) site, but do not show this dipole contribution either, and find only a charge redistribution from Cu(2) $d_{x^2-y^2}$ into d_{z^2} orbitals.

Because earlier X-ray experiments using photons of lower energies suffered from absorption and extinction problems, it is difficult to compare the present results with those from literature. For example, Sasaki *et al.* (1992) refined their data to $R(F) = 0.018$, Buttner *et al.* (1992) to $R(F) = 0.04$ and Jang *et al.* (1996) to 0.026, respectively, all using the IAM only. The first authors investigated a crystal of lower oxygen content, i.e. with a tetragonal structure, and they found a spherical charge-density distribution at Cu(1) and some density accumulations along the c axis, which were not reproduced by our results. On the other hand, they reported the presence of a $d_{x^2-y^2}$-type hole at Cu(2), which was also found by our investigation. Interestingly, the features in their residual density maps near the Ba ion resembled those found in our deformation densities, but they were able to reduce these residual densities using higher-order tensors for anharmonic thermal vibrations.

The charge-density maps of Buttner *et al.* (1992) agree qualitatively in some aspects with our results. These authors also found charge depletions between the Cu and O atoms. Especially, the charge-density polarization of Cu(2) along **c** is well reproduced, *i.e.* with depletion towards O(4) and accumulation towards the adjacent copper. Differences, however, were found in the (001) plane at $z = 0$ but these might be ascribed to the presence of oxygen on the O(5) site in their crystal, which was definitively absent in our sample. A further difference was found along the Cu(2)—O(4) bond. The small density accumulation they found was not reproduced in our results.

The best agreement was found comparing our results to those of Jang *et al.* (1996) performed on a detwinned $YBa_2Cu_3O_{6.98}$ crystal. Although the authors did not perform multipole refinements, their Fourier difference maps show some remarkably similar features compared with our deformation densities, *i.e.* no density along the Cu—O bonds, no density at the O(5) site, a polarization of Cu(2) with a lone pair along the *c* axis on the opposite side of O(4) and a significant deformation density near Ba. In contrast to our results, however, the authors reported a polarization of O(2) and no polarization of O(3).

10. Conclusions

A striking conclusion of this study is that theoretical and experimental results match surprisingly well. Although there are some differences in the details of the densities, the principal features were represented in both cases.

Moreover, the experimental results presented above clearly show that high-energy synchrotron radiation is an excellent tool to study structures containing heavy elements. High-energy radiation of sufficient intensity now opens the gate to structures that could not be precisely examined in the past owing to massive vitiations by absorption and extinction problems.

With respect to the (in most cases excellent) agreement between theory and experiment, it is now possible to compare high-T_c superconductor charge densities both qualitatively and quantitatively, which should allow us to improve the models and to yield even better agreements of theory and experiment. In agreement with the general consensus that the holes in the O(2)—Cu(2)—O(3) planes leading to superconductivity are located between Cu and O, we find electron depletions in these bonds. Analyses of the charge-transfer properties will be published in a forthcoming paper. Furthermore, the experimental investigations will be expanded to *e.g.* oxygen-deficient samples and to further high-T_c superconductor structures in the near future.

The statements concerning ionicity of the bonds in YBCO presented in this paper are based on a topological analysis of the charge density. As recently shown by Raub & Jansen (2001), a better approach is possible using a combination of the analysis of the density and the electron localization function, but one should mention here that this technique requires some approximations if experimental densities are to be investigated. Thus, in a forthcoming contribution, we intend to continue the ionicity discussion by further analyses of AIM integral properties.

References

Andersen, N., Lebech, B. & Poulsen, H. (1990). *Physica (Utrecht)*, C**172**, 31–42.

Bader, R. (1990). *Atoms in Molecules: a Quantum Theory*. Oxford: Clarendon Press.

Bader, R. (1998). *J. Phys. Chem. A*, **102**, 7314–7323.

Bader, R. & Essen, H. (1984). *J. Chem. Phys.* **80**, 1943–1960.

Becker, P. & Coppens, P. (1974). *Acta Cryst.* A**30**, 129–147.

Blaha, P., Novak, P. & Schwarz, K. (2002). Unpublished results.

Blaha, P., Schwarz, K., Madsen, G., Kvasnicka, D. & Luitz, J. (2001). *WIEN2k, An Augmented Plane Wave + Local Orbitals Program for Calculating Crystal Properties*. K. Schwarz, TU Wien. ISBN 3-9501031-1-2.

Bouchard, R., Hupfeld, D., Lippmann, T., Neuefeind, J., Neumann, H.-B., Poulsen, H., Rütt, U., Schmidt, T., Schneider, J., Süssenbach, J. & von Zimmermann, M. (1997). *J. Synchrotron Rad.* **5**, 90–101.

Buttner, R. & Maslen, E. (1992). *Acta Cryst.* B**48**, 644–649.

Buttner, R., Maslen, E. & Spadaccini, N. (1992). *Acta Cryst.* B**48**, 21–30.

Bytheway, I., Chandler, G. & Figgis, B. (2002). *Acta Cryst.* A**58**, 451–459.

Casalta, H., Schleger, P., Harris, P., Lebech, B., Andersen, N., Liang, R., Dosanjh, P. & Hardy, W. (1996). *Physica (Utrecht)*, C**258**, 321–330.

Chandler, C. (1995). *J. Phys. Chem. Ref. Data*, **24**, 71–643.

Clementi, E. (1965). *IBM J. Res. Dev.* **9** (Suppl.).

Clementi, E. & Roetti, C. (1974). *At. Data Nucl. Data Tables*, **14**, 177–478.

Eichhorn, K. (1982). *TDSCOR. TDS-Correction of Integrated Intensities from Single Crystals*. FR Kristallographie, Universität des Saarlandes, Saarbrücken, Germany.

Flensburg, C. (2000). Private communication.

Flensburg, C. & Madsen, D. (2000). *Acta Cryst.* A**56**, 24–28.

Hamilton, W. (1969). *Acta Cryst.* A**25**, 194–206.

Hansen, N. & Coppens, P. (1978). *Acta Cryst.* A**34**, 909–921.

Howard, S., Hursthouse, M., Lehmann, C. & Poyner, E. (1995). *Acta Cryst.* B**51**, 328–337.

Jang, W.-J., Mori, H., Watahiki, M., Tajima, S., Koshizuka, N. & Tanaka, S. (1996). *J. Solid State Chem.* **122**, 371–375.

Johnson, C. (1969). *Acta Cryst.* A**25**, 187–194.

Kendal, M. & Stuart, A. (1958). *The Advanced Theory of Statistics*. London: Griffin.

King, H. & Finger, L. (1979). *J. Appl. Cryst.* **12**, 374–378.

Kirfel, A., Gupta, A. & Will, G. (1979). *Acta Cryst.* B**35**, 2291–2300.

Kirfel, A., Krane, H.-G., Blaha, P., Schwarz, K.-H. & Lippmann, T. (2001). *Acta Cryst.* A**57**, 663–677.

Koga, T., Watanabe, S., Kanayama, K., Yasuda, R. & Thakkar, A. (1995). *J. Chem. Phys.* **103**, 3000–3005.

Lippmann, T. (2002). http://www-hasylab.desy.de/science/groups/schneider_group/ecds/ecds.html.

Lippmann, T. & Schneider, J. (2000*a*). *J. Appl. Cryst.* **33**, 156–167.

Lippmann, T. & Schneider, J. (2000*b*). *Acta Cryst.* A**56**, 575–584.

Luana, V., Costales, A. & Pendas, A. (1997). *Phys. Rev. B*, **55**, 4285–4297.

Madsen, G., Blaha, P., Schwarz, K.-H., Sjostedt, E. & Nordstrom, L. (2001). *Phys. Rev. B*, **64**, 195134/1–195134/9.

Menon, C. & Eldhose, N. (1992). *Solid State Commun.* **81**, 357–359.

Morse, M. & Cairns, S. (1969). *Critical Point Theory in Global Analysis and Differential Geometry.* New York: Academic Press.

Novak, P., Boucher, F., Gressier, P., Blaha, P. & Schwarz, K. (2001). *Phys. Rev. B*, **63**, 235114-1–235114-8.

Pendas, A., Costales, A. & Luana, V. (1997). *Phys. Rev. B*, **55**, 4275–4284.

Perdew, J. & Wang, Y. (1992). *Phys. Rev. B*, **45**, 13244.

Pickett, W. (1989). *Rev. Mod. Phys.* **61**, 433–512.

Poulsen, H. & Neuefeind, J. (1995). *Nucl. Instrum. Methods*, B**95**, 509–514.

Raub, S. & Jansen, G. (2001). *Theor. Chem. Acc.* **106**, 223–232.

Rees, B. (1978). *Acta Cryst.* A**34**, 254–256.

Sasaki, S., Inoue, Z., Iyi, N. & Takekawa, S. (1992). *Acta Cryst.* B**48**, 393–400.

Schwarz, K.-H., Ambrosch-Draxl, C. & Blaha, P. (1990). *Phys. Rev. B*, **42**, 2051.

Schwarz, K.-H. & Blaha, P. (1996). *Lecture Notes in Chemistry*, **67**, 139.

Sofo, J. & Fuhr, J. (2001). *AIM Program for Wien.* Inst. Balseiro, Bariloche, Argentina.

Stevens, E. & Coppens, P. (1975). *Acta Cryst.* A**31**, 612–619.

Stevens, E. & Coppens, P. (1976). *Acta Cryst.* A**32**, 915–917.

Stewart, R. (1969). *J. Chem. Phys.* **51**, 4569–4577.

Stewart, R., Spackman, M. & Flensburg, C. (2000). *VALRAY Users Manual*, 2nd ed. Department of Chemistry, Carnegie-Mellon University, Pittsburgh, PA 15213, USA, and University of Copenhagen, Denmark.

Sullivan, J., Bordet, P., Marezio, M., Takenaka, K. & Uchida, S. (1993). *Phys. Rev. B*, **48**, 10638–10641.

Thakkar, A. (2001). http://www.unb.ca/Chem/ajit/f_download.htm.

Volkov, A., Abramov, Y., Coppens, P. & Gatti, C. (2000). *Acta Cryst.* A**56**, 332–339.

Wolf, T. (1996). *J. Cryst. Growth*, **166**, 810–815.